Conformational changes of a membrane protein determined by infrared difference spectroscopy beyond the diffraction limit

Raffaella Polito,[1,†] Maria Eleonora Temperini,[1,2,†] Eglof Ritter,[3,4] Ljiljana Puskar,[3] Ulrich Schade,[3] Matthias Broser,[4] Peter Hegemann,[4] Leonetta Baldassarre,[1] Michele Ortolani,[1] and Valeria Giliberti[2,*]

[1] *Department of Physics, Sapienza University of Rome, Piazzale Aldo Moro 2, I-00185 Roma, Italy*
[2] *Istituto Italiano di Tecnologia, Center for Life NanoScience, Viale Regina Elena 291, I-00161 Roma, Italy*
[3] *Helmholtz-Zentrum Berlin für Materialien und Energie GmbH, Albert-Einstein-Str. 15, 12489 Berlin, Germany*
[4] *Humboldt-Universität zu Berlin, Institut für Biologie, Invalidenstraße 42, D-10115 Berlin, Germany*

(Received 11 April 2021; revised 15 June 2021; accepted 29 June 2021; published 20 July 2021)

Optogenetics is a revolutionary method for studying neural activity by exploiting the optical stimulation of neurons made possible by artificial genetic expression of light-sensitive transmembrane "gate" proteins. Evidence of functional conformational changes of the gate proteins can be obtained by difference infrared (IR) absorption spectroscopy triggered by light stimuli. Here we investigate the effect on the photocycle of the prototype optogenetic protein channelrhodopsin (ChR2) of gold surfaces placed in close proximity to the protein molecules. In order to do this, we bring difference IR spectroscopy to the nanoscale, using a platform based on the coupling of a tunable mid-IR quantum cascade laser and an atomic force microscope (AFM). Sensitivity to individual subwavelength-sized membrane patches, embedding fewer than a hundred ChR2 molecules, is achieved by taking advantage of a plasmonic field enhancement in the nanogap between the gold-coated AFM tip and an ultraflat gold surface used as a sample support. We obtain relative difference absorption variations smaller than 10^{-2} and benchmark nanospectroscopy difference spectra against those taken with the Fourier transform IR (FTIR) spectroscopic technique on the same sample. We identify distinct simultaneous processes in the ChR2 photocycle by performing singular value decomposition of the FTIR difference spectra, and use this procedure to compare IR nanospectroscopy data on individual membrane patches in contact with gold surfaces with those obtained on thick stacks of membrane patches unexposed to metal surfaces. ChR2 proteins maintain their gate function when placed in a 14-nm-wide gap between two gold surfaces, apart from minor modifications to their kinetics. Our results are relevant to optogenetic applications that require physical contact between nanoscale metallic probes and electrodes and the membrane of single neuronal cells. More generally, our work paves the way towards the spectroscopic study of transmembrane proteins at the nanoscale.

DOI: 10.1103/PhysRevApplied.16.014048

I. INTRODUCTION

Optogenetics, exploiting the temporal and spatial precision of optical beams to remotely control genetically modified cells [1], represents a revolutionary and promising tool for understanding neural activity [2,3]. The control of electrically excitable cells, including neurons, is achieved by genetic expression of light-sensitive transmembrane proteins (TMPs) that, under illumination with visible light at specific wavelengths, undergo a cyclic sequence of conformational changes (also referred to as the protein photocycle), opening and closing "gates" for ion transport through the cell membrane of their hosts [4]. Although optogenetics is undoubtedly a powerful technique, numerous scientific and technical challenges are yet to be met before this tool can be routinely used for the *in vivo* study of the correlation between the neural activity and the observed behavior of living organisms [1,5–8].

In order to achieve a precise spatial-temporal interface with the neurons for light delivery and electrical signal readout, an optogenetic setup typically requires close contact between the cell membrane and the miniaturized probes and electrodes. One biophysics question worthy of being addressed is whether there is an effect on the light-sensitive TMP functions of proximal metal surfaces: in several of the proposed *in vivo* optogenetic techniques, indeed, metal electrodes or metal-coated optical fibers are typically put in direct contact with the cell membrane [7–9], and it has been reported that these configurations

*valeria.giliberti@iit.it
†These authors contributed equally to the work.

can alter or even hamper the TMP photocycle [10,11]. A method of analysis of the detailed conformational changes of TMPs at the single neuron level, often required to understand the optogenetic gate function, is still lacking. Time-resolved optical spectroscopies, in particular Fourier transform IR (FTIR) absorption spectroscopy at mid-IR wavelengths between 5 and 20 μm, can elucidate the sequence of molecular mechanisms of light-sensitive proteins [12,13]. However, the diffraction limit prevents the mid-IR investigation of TMPs in individual intact cells or even in artificially reconstituted lipid membrane patches.

In this work, we study the functional conformational changes of the light-gated ion channel Channelrhodopsin-2 (ChR2) [6], the most widely used optogenetic tool, by taking advantage of the IR nanospectroscopic approach based on the coupling of mid-IR lasers to atomic force microscopes (AFMs) [14–17]. Among several IR nanospectroscopic methods [18–23], here we use the photothermal expansion method, hereafter called AFM-IR [20,21], with which we recently reported on IR difference nanospectroscopy of the prototype TMP bacteriorhodopsin (BR) [17]. The experimental configuration of a membrane patch sandwiched between a gold-coated AFM tip and a gold surface represents the ideal scenario to investigate the effect of a metal surface put in direct physical contact with the cell membrane.

II. RESULTS AND DISCUSSION

A. AFM-IR of individual membrane patches

The AFM-IR technique exploits photothermal expansion as measured by the AFM readout circuit [24]. As a result of the absorption of IR radiation emitted by a laser at a specific wavelength, a molecule goes into an excited vibrational state and then dissipates the energy nonradiatively via vibrational modes of lower energy. Because of the anharmonicity of the potential, there is an effective increase of the molecule's volume, which is recorded by the cantilever oscillation. The local IR absorption spectrum is obtained by monitoring the amplitude of the cantilever oscillation upon tuning the IR wavelength (see Supplemental Material S1 for experimental details [25]). Our samples consist of lipid membrane assemblies of different thickness (hereafter called self-assemblies), containing the "slow mutant" of ChR2, named C128S [26], deposited on ultraflat template-stripped gold chips. It has been demonstrated, and here further corroborated by electromagnetic simulations, that the use of a micrometer-long gold-coated AFM tip acting as a plasmonic antenna at IR frequencies, in combination with a gold surface used as a support of nanometer-thick samples, produces a strong field enhancement in the mid-IR range, which is localized in the sample volume below the tip. The combination of this plasmonic nanogap configuration with the resonantly enhanced acquisition mode provided by the use of a quantum cascade laser (QCL), in which the amplitude of the cantilever oscillation is resonantly amplified due to the matching of the laser repetition rate with the cantilever bending mode, allows one to measure the photothermal expansion of few-nanometer-thick samples that otherwise would be below the AFM sensitivity [14,15,17]. Self-assemblies sandwiched between the gold-coated AFM tip and the ultraflat gold surface are here used for the spectroscopic investigation of light-sensitive proteins under controlled morphological and electromagnetic conditions, a key condition for the unambiguous interpretation of the IR data [12,17]. For completeness, we mention that other methods based on the combination of an AFM and an IR laser, such as scattering-type microscopy [27] and photoacoustic spectroscopy [28], may also be suitable to obtain similar nanospectroscopic information [24].

In Fig. 1(a) (left panel) we report the AFM topographic map of a representative self-assembly containing ChR2, which consists for a large portion of a single membrane patch (thickness around 7 nm), while on the left-hand side there is an overlap of two and even three membrane patches. In Fig. 1(b) (left panel), for comparison, we show the AFM topographic map acquired on a single native purple membrane patch containing the prototype light-sensitive protein BR. The homogeneity of the membrane patches in terms of protein embedding is demonstrated by the AFM-IR spatial maps in the right panels of Figs. 1(a) and 1(b). As reported in the Supplemental Material S2 [25], the possibility of correlating mechanical and spectroscopic properties, which is characteristic of AFM-IR nanoimaging, allows also to discard non-membrane-shaped lipid aggregates, a common occurrence in artificial samples, and select only intact membrane patches (TMPs often lose or change their activity when removed from the lipid environment [29]).

The AFM-IR spectra acquired on ChR2- and BR-containing membranes of different thickness are plotted in Fig. 1(c). In agreement with FTIR results [30] (see also Supplemental Material S3 [25]), the AFM-IR spectra obtained on ChR2 samples show the two amide bands associated with the vibrations along the protein backbone of the mostly helical structure of ChR2 (the amide-I peak at 1660 cm^{-1}, related to C=O stretching, and the amide-II peak at 1550 cm^{-1}, related to N—H bending) [31]. A less intense band is found around 1740 cm^{-1}, related to the C=O stretching of the lipid—ester bonds [32], which are present in eukaryote cells that express ChR2, but not in *archaea* (the class of organisms to which purple membranes belong) that express BR [33]. The high degree of vertical orientation of ChR2 molecules in our artificial membrane patches is confirmed by the fact that the amide-I and amide-II bands display the same peak frequency and comparable relative intensity in all spectra of Fig. 1(c) (apart from the nonstacked 150-nm-thick assembly). For

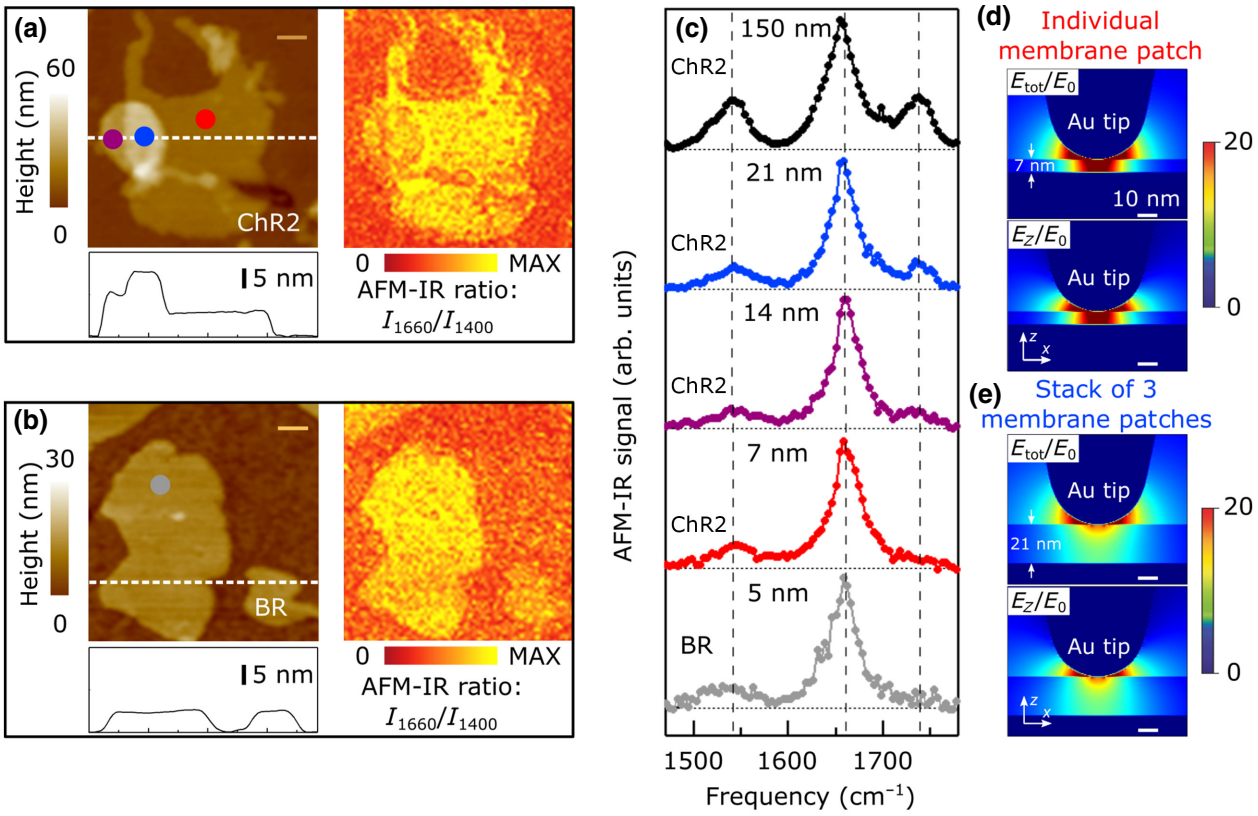

FIG. 1. (a) and (b) Left: AFM topographic map and line profile of self-assemblies containing either ChR2 (a) or BR (b). The scale bar is 100 nm. Right: AFM-IR ratio maps I_{1660}/I_{1400} obtained by dividing the map acquired at 1660 cm^{-1} (amide-I band) by the map acquired at 1400 cm^{-1} (any IR absorption of the membrane). (c) AFM-IR spectra obtained at different locations of the ChR2-containing self-assembly and on the individual purple membrane. (d) and (e) Simulated maps of electric field modulus E_{tot} (top panels) and electric field z component normal to the gold surface E_z (bottom panels) normalized by the electric field modulus of the incident beam E_0, for an individual membrane patch (d) and a stack of three lipid membrane patches (e) containing ChR2.

reference, full vertical orientation of the BR-containing membrane patches has been verified previously [17], and full orientation of ChR2-containing patches is therefore assumed by analogy considering that the two proteins share the prototypical secondary structure of rhodopsins consisting of seven transmembrane helices, with the same helix orientation [4]. The electromagnetic simulations of Figs. 1(d) and 1(e) show a fully vertical, i.e., z-oriented, electric field orientation in films of thickness up to 21 nm. Moreover, the line profile reported in Fig. 1(a) confirms an oriented stacking of the membrane patches in units of single membrane thickness of 7 nm (ChR2 assemblies up to 21 nm thickness, i.e., up to three stacked membranes have been observed). Therefore, the orientation of the ChR2 molecules in our artificial lipid membrane patches is comparable to that of BR proteins in native purple membranes.

B. AFM-IR difference nanospectroscopy

We then use the AFM-IR platform to perform a functional study of ChR2 by probing its light-activated conformational changes connected to the ion channel function (see Supplementary Material S1 for experimental details [25]). The retinal chromophore of ChR2, which is covalently linked to one of the seven helices of the protein spanning the lipid membrane, undergoes a photoisomerization from all-*trans* to 13-*cis* upon blue light absorption (maximum absorption at 470 nm) that, in turn, causes a cyclic sequence of conformational changes (the protein photocycle), resulting in the opening of the channel gate and consequent passive flow of cations. Under stationary light illumination conditions, present in our experiments as well as in several optogenetic applications, the photocycle of ChR2 increases in complexity due to secondary photoreactions. Such secondary photoreactions originate from the coexistence of two parallel photocycles with 13-*cis*,C = N-*anti* and 13-*cis*,C = N-*syn* retinal conformations, in contrast to single-turnover conditions in which proteins are excited by a short light pulse and the retinal adopts the 13-*cis*,C = N-*anti* conformation only [34,35]. In Fig. 2(a) we report a simplified four-state model adapted from the ChR2 photocycle recently proposed by Kuhne *et al.* in Ref. [13] as a unifying model describing

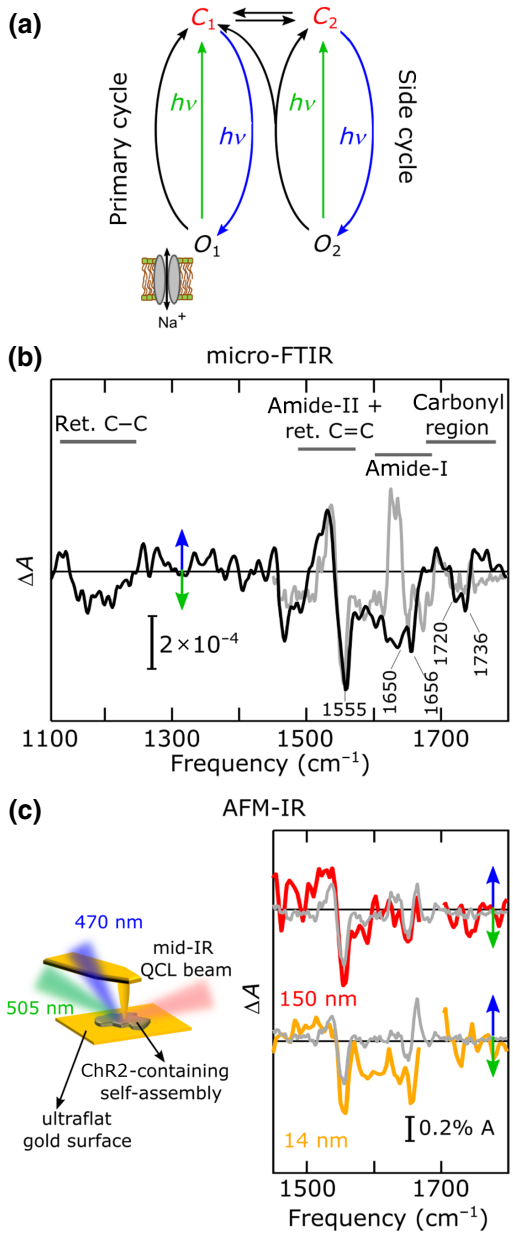

FIG. 2. (a) Four-state photocycle model which consists of a primary cycle (dark closed state C_1 and open conductive state O_1 for Na^+ ions) and a side cycle (dark closed state C_2 and open conductive state O_2). Blue light initiates the photocycle. The C_1 and C_2 states can be accessed directly from O_1 and O_2 with green light. The photon energy is indicated by $h\nu$, where ν is the photon electromagnetic frequency and h the Planck's constant. The black arrows indicate the thermal relaxation between the states. (b) Micro-FTIR ΔA obtained on a micrometer-thick area of a ChR2 self-assembly deposited on an ultraflat gold surface. C−C and C = C labels represent single and double bonds of the carbon atoms, respectively. (c) AFM-IR ΔA obtained on 150-nm-thick and 14-nm-thick areas of ChR2 self-assemblies deposited on an ultraflat gold surface. Gray curves in panels (b) and (c) are the best fit defined as a linear combination of the three independent spectral components ΔA_{helix}, $\Delta A_{\text{sidecyc}}$, and ΔA_{gate} of Fig. 3.

both single-turnover experiments and recordings under continuous illumination. The protein conformational changes that characterize the intermediate states of the photocycle result in modifications of the line shape and of the central frequency of most IR absorption bands, which can then be probed by measuring the IR absorption difference between the spectrum acquired under visible illumination that activates the proteins, and the spectrum acquired in dark conditions. Here we obtain a significant improvement of the signal-to-noise ratio of the AFM-IR difference spectra, required to probe small light-induced absorption variations falling in the range 10^{-3}–10^{-5} [12], thanks to the field enhancement in the plasmonic nanogap between the gold-coated AFM probe tip and the ultraflat gold surface. In addition, following an experimental protocol that we have recently pioneered and validated on the more common protein BR [17], we also average many spectra acquired during the on-off reproducible photocycle of ChR2. This is made possible here by the use of the slow mutant of ChR2 named C128S, in which a substitution of the amino acid cysteine in position 128 (Cys128) with a nonpolar amino acid removes a disulfide bridge from the molecule and this is known to "block" the protein in the open intermediate state [O_1 in Fig. 2(a)], which can be overcome with green light illumination. This effect enables an on-off switching of the ChR2 channel gate by alternating blue and green light [26].

In Figs. 2(b) and 2(c), the AFM-IR difference spectra obtained on ChR2 self-assemblies of thickness 150 nm and 14 nm are compared with the micro-FTIR difference spectrum obtained on a different portion of the same gold support where the protein assembly thickness is larger than 1 μm and therefore not fewer than 10^7 proteins are probed. We focus on stacks of two-membrane patches (thickness of 14 nm), instead of monolayers, because we experimentally observe that prolonged contact-mode AFM measurements of the 7-nm-thick single membrane patches yield physical degradation of the self-assembly. The difference spectra are calculated as $\Delta A = A_{\text{blue}}(\omega) - A_{\text{green}}(\omega)$, where $A_{\text{blue}}(\omega)$ and $A_{\text{green}}(\omega)$ are the spectra acquired, either by AFM-IR or micro-FTIR, under blue and green light, at 470 nm and 505 nm, respectively, provided by exactly the same visible-light-emitting-diode illumination setup. The micro-FTIR ΔA on the micrometer-thick assembly is used as a benchmark for AFM-IR data taken on nanometer-thick self-assemblies. According to the model in Fig. 2(a), the positive bands of our experimental difference spectra ΔA mainly represent vibrations of a mixture of the open O_1 and O_2 states reached under blue illumination, while the negative bands can be assigned to vibrations of a mixture of the closed C_1 and C_2 states obtained under green illumination. By comparing our spectra in Figs. 2(b) and 2(c) with the FTIR difference spectra of the O_1 and O_2 states reported by Kuhne *et al.* [13], we find that our micro-FTIR ΔA spectrum

shows spectral features of both the primary and the side cycle. The feasibility of probing the light-induced ChR2 conformational changes by AFM-IR is finally demonstrated by the good agreement between the micro-FTIR ΔA and the AFM-IR ΔA spectra acquired on the 150-nm-thick ChR2 sample [Fig. 2(c)]. Most of the main spectral features, including the sharp C=C retinal stretching vibration peak (around 1555 cm^{-1}) and the two negative peaks in the carbonyl region around 1720 cm^{-1} and 1736 cm^{-1}, are indeed also present in the AFM-IR ΔA difference spectrum [36,37]. The AFM-IR ΔA spectrum acquired on a 14-nm-thick ChR2 self-assembly (stack of two membrane patches) shows the main spectral features of the ChR2 conformational changes with relative absorption variations smaller than 10^{-2}, confirming the photoactivation of ChR2 molecules in direct contact with gold surfaces. A dramatic decrease in the number of probed molecules compared to FTIR spectroscopy is demonstrated: under strong plasmonic field enhancement, the sample volume that generates the AFM-IR photothermal expansion signal corresponds to a cylinder located below the AFM tip apex [14,15,17], which contains approximately 120 ChR2 proteins (see Supplemental Material S4 for the details of this calculation [25]), while a FTIR liquid cuvette can easily contain 10^{10} molecules.

In order to isolate and understand the effect of protein proximity to gold surfaces, we now compare our micro-FTIR and AFM-IR ΔA spectra obtained on micrometer-thick, 150-nm-thick and 14-nm-thick assemblies, using conventional FTIR data obtained on the same sample in a liquid cuvette as reference ΔA spectra. Time-dependent sets of absorbance spectra are recorded before illuminating the sample with visible light, during alternating illumination with light at the two different wavelengths (blue and green), and after the visible illumination is turned off. Difference spectra are calculated by subtraction of a reference spectrum representing the state before the start of the illumination protocol from the whole set. Sets of difference spectra are then normalized using bands in the ethylenic region and/or fingerprint region [34]. The data sets are analyzed by singular value decomposition followed by a rotation procedure that, as described previously [38], allows one to calculate the spectral features following the same course of time. By adopting this method, we calculate the superimposed contributions of the different simultaneous processes to obtain the pure kinetics and the spectral contributions of the three independent processes. Figure 3 shows the reference ΔA spectra [Figs. 3(a), 3(c) and 3(e)] and relative kinetics [Figs. 3(b), 3(d) and 3(f)] calculated from conventional FTIR experiments. The first component mainly reflects adjustment of residues along the protein backbone, i.e., the helices. The second component represents a parasitic "side photocycle" characterized by a less conductive open state [13], as hinted from its reaction kinetics described in detail in the

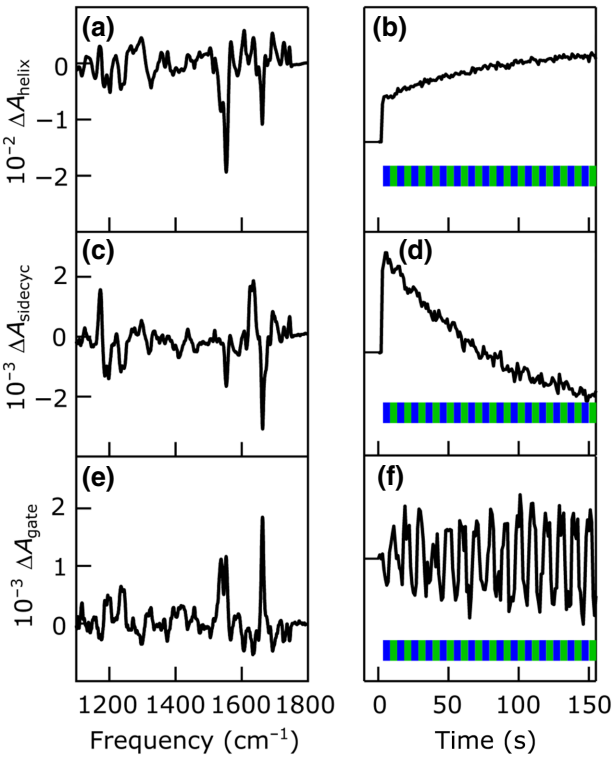

FIG. 3. Base spectral components [(a), (c), and (e)] and relative kinetic [(b), (d), and (f)] of the three independent spectral contributions characterizing the FTIR kinetic data of C128S during alternating blue and green illuminations. Singular value decomposition and rotation procedure are adopted to calculate the three components from the time-resolved FTIR data set.

Supplemental Material S5 [25]. The third component can be identified with the cyclic process of opening and closing the internal transmembrane channel gate [34]. We therefore refer to the corresponding three difference spectra as ΔA_{helix}, $\Delta A_{sidecyc}$, and ΔA_{gate}. We then fit to the experimental micro-FTIR and AFM-IR ΔA curves of Figs. 2(b) and 2(c) the following expression:

$$\Delta A = c_{helix}\Delta A_{helix} + c_{sidecyc}\Delta A_{sidecyc} + c_{gate}\Delta A_{gate},$$

where c_{helix}, $c_{sidecyc}$, and c_{gate} are the best-fit linear combination coefficients. One can observe a good agreement between the experimental and the fitting curves [gray curves in Figs. 2(b) and 2(c)], the main differences being the positive band at around 1640 cm^{-1} present only in the fitting curves, which may be due to the different hydration levels in the FTIR experiment with the sample in a liquid cuvette, and the micro-FTIR and AFM-IR experiments with the sample drop-cast on a metal surface and allowed to dry in air [15]. In contrast with c_{helix} and c_{gate}, the coefficient $c_{sidecyc}$ decreases with the thickness t, between $t > 1000$ nm and $t = 150$ nm (see Table I). This result suggests a dependence of the ChR2 photocycle branching ratio

TABLE I. Absolute value of the best-fit linear combination coefficients c_{helix}, c_{sidecyc}, and c_{gate}.

	c_{helix}	c_{sidecyc}	c_{gate}
Micro-FTIR $t > 1000$ nm	0.017	0.15	0.33
AFM-IR $t = 150$ nm	0.022	0.07	0.30
AFM-IR $t = 14$ nm	0.022	0.03	0.28

on the thickness. In particular, the reduction of c_{sidecyc} with t hints towards the reduction in the probability of entering the parasitic side cycle for proteins that are in close proximity to gold surfaces. This effect can be ascribed to the proximity with metal surfaces, since micro-FTIR and AFM-IR samples are in the same form; also, regarding protein hydration, the main effect upon decreasing sample thickness is the increase in the number of proteins that are in contact with gold surfaces (ideally 100% in the 14-nm-thick sample). Our result could be exploited to increase the efficiency of optogenetic gates by purposely approaching them with metal surfaces, e.g., with metal nanoparticles that can be safely bound to neurons even in *in vivo* experiments. In any case, we can confirm the proper light-induced functional activation of ChR2 gates when the proteins are put in direct contact with the gold surfaces.

It remains to be understood how the adhesion or proximity to metal surfaces can impact on the protein functions. From the plasmonic point of view, one can consider that the main effect in the mid-IR range is the enhancement of the field intensity. Plasmonic effects of heat generation due to absorption of gold can be neglected since the temperature increase is expected to be very low, as also confirmed by thermal simulations previously reported [17], while plasmonic-assisted charge transfer can be ruled out at IR frequencies due to the low photon energy. Finally, one can safely exclude the hypothesis of strong interaction that is known to produce a redistribution of the spectral weight in the molecular vibrational spectrum [39], due to the high losses of our plasmonic cavity [40] that place our system out of the strong light-matter coupling condition, although marginally. To conclude, one possible mechanism underlying the decrease of the side cycle probability with decreasing thickness of the self-assemblies can be an alteration of the membrane surface potential. Contact with metal surfaces may indeed yield charge redistribution between the two faces of the membrane patches, which in turn can result in a variation of the branching ratio [13]. Further experimental measurements would be necessary to validate this interpretation. However, in our AFM-IR experiments we still do not have any control of the membrane potential, although we can envision a combination of the spectroscopic capabilities of AFM-IR with the well-established electrical measurement capabilities of conducting-scanning probes on protein monolayers.

III. CONCLUSIONS

We demonstrate that the IR nanospectroscopic technique based on the photoexpansion effect, AFM-IR, can be used to push IR difference spectroscopy of protein conformational changes well beyond the diffraction limit. Here we study one of the most important proteins used in optogenetic applications, the light-sensitive transmembrane protein channelrhodopsn ChR2, by combining AFM-IR with the plasmonic field enhancement in the nanogap between a gold-coated AFM tip and an ultraflat gold surface used as a support for the individual artificially reconstituted lipid membrane patches embedding the ChR2 molecules. We probe relative light-induced absorption variations smaller than 10^{-2}, averaging over 10^2 membrane proteins only. This result represents a significant improvement of the sensitivity for the IR functional study of proteins, since conventional IR experimental configurations require not less than 10^6 protein molecules to generate a difference spectroscopy signal. By benchmarking the AFM-IR difference spectra against those acquired by conventional IR spectroscopy on the same sample measured in a liquid cuvette, we obtain evidence that proteins in proximity to gold surfaces may show a reduced probability of entering the known parasitic side cycle characterized by a less conductive open state. This result points towards higher efficiency in the conversion of light into charge transfer for proteins adhering to metal surfaces, a configuration that could purposely be engineered to increase the efficiency of optogenetic gates.

ACKNOWLEDGMENTS

Authors acknowledge the contribution of Paolo Biagioni for the electromagnetic simulations reported in Fig. 1.

[1] A. M. Packer, B. Roska, and M. Häusser, Targeting neurons and photons for optogenetics, Nat. Neurosci. **16**, 805 (2013).
[2] K. Deisseroth, Optogenetics, Nat. Methods **8**, 26 (2011).
[3] L. Fenno, O. Yizhar, and K. Deisseroth, The development and application of optogenetics, Annu. Rev. Neurosci. **34**, 389 (2011).
[4] O. P. Ernst, D. T. Lodowski, M. Elstner, P. Hegemann, L. S. Brown, and H. Kandori, Microbial and animal rhodopsins: Structures, functions, and molecular mechanisms, Chem. Rev. **114**, 126 (2014).
[5] M. Grote, M. Engelhard, and P. Hegemann, Of ion pumps, sensors and channels—perspectives on microbial rhodopsins between science and history, Biochim. Biophys. Acta, Bioenerg. **533**, 1837 (2014).
[6] F. Schneider, C. Grimm, and P. Hegemann, Biophysics of channelrhodopsin, Annu. Rev. Biophys. **44**, 167 (2015).

[7] S. Chen, W. Pei, Q. Gui, Y. Chen, S. Zhao, H. Wang, and H. Chen, A fiber-based implantable multi-optrode array with contiguous optical and electrical sites, J. Neural Eng. **10**, 046020 (2013).

[8] F. Pisanello, L. Sileo, I. A. Oldenburg, M. Pisanello, L. Martiradonna, J. A. Assad, B. L. Sabatini, and M. De Vittorio, Multipoint-emitting optical fibers for spatially addressable in vivo optogenetics, Neuron **82**, 1245 (2014).

[9] B. Fan and W. Li, Miniaturized optogenetic neural implants: A review, Lab Chip **15**, 3838 (2105).

[10] T. He, N. Friedman, D. Cahen, and M. Sheves, Bacteriorhodopsin monolayers for optoelectronics: Orientation and photoelectric response on solid supports, Adv. Mater. **17**, 1023 (2005).

[11] S. Mukhopadhyay, S. R. Cohen, D. Marchak, N. Friedman, I. Pecht, M. Sheves, and D. Cahen, Nanoscale electron transport and photodynamics enhancement in lipid-depleted bacteriorhodopsin monomers, ACS Nano **8**, 7714 (2014).

[12] V. A. Lorenz-Fonfria, Infrared difference spectroscopy of proteins: From bands to bonds, Chem. Rev. **120**, 3466 (2020).

[13] J. Kuhne, J. Vierock, S. A. Tennigkeit, M. A. Dreier, J. Wietek, D. Petersen, K. Gavriljuk, S. F. El-Mashtoly, P. Hegemann, and K. Gerwert, Unifying photocycle model for light adaptation and temporal evolution of cation conductance in channelrhodopsin-2, Proc. Natl. Acad. Sci. U. S. A. **116**, 9380 (2019).

[14] F. Lu, M. Jin, and M. A. Belkin, Tip-enhanced infrared nanospectroscopy via molecular expansion force detection, Nat. Photonics **8**, 307 (2014).

[15] V. Giliberti, M. Badioli, A. Nucara, P. Calvani, E. Ritter, L. Puskar, E. F. Aziz, P. Hegemann, U. Schade, M. Ortolani, and L. Baldassarre, Heterogeneity of the transmembrane protein conformation in purple membranes identified by infrared nanospectroscopy, Small **13**, 1701181 (2017).

[16] S. Berweger, D. M. Nguyen, E. A. Muller, H. A. Bechtel, T. T. Perkins, and M. B. Raschke, Nano-chemical infrared imaging of membrane proteins in lipid bilayers, J. Am. Chem. Soc. **135**, 18292 (2013).

[17] V. Giliberti, R. Polito, E. Ritter, M. Broser, P. Hegemann, L. Puskar, U. Schade, L. Zanetti-Polzi, I. Daidone, S. Corni, F. Rusconi, P. Biagioni, L. Baldassarre, and M. Ortolani, Tip-enhanced infrared difference-nanospectroscopy of the proton pump activity of bacteriorhodopsin in single purple membrane patches, Nano Lett. **19**, 3104 (2019).

[18] F. Keilmann and R. Hillenbrand, Near-field microscopy by elastic light scattering from a tip, Philos. Trans. R. Soc., A **362**, 787 (2004).

[19] F. Huth, A. Govyadinov, S. Amarie, W. Nuansing, F. Keilmann, and R. Hillenbrand, Nano-FTIR absorption spectroscopy of molecular fingerprints at 20 nm spatial resolution, Nano Lett. **12**, 3973 (2012).

[20] A. M. Katzenmeyer, G. Holland, J. Chae, A. Band, K. Kjoller, and A. Centrone, Mid-infrared spectroscopy beyond the diffraction limit via direct measurement of the photothermal effect, Nanoscale **7**, 17637 (2015).

[21] A. Dazzi and C. B. Prater, AFM-IR: Technology and applications in nanoscale infrared spectroscopy and chemical imaging, Chem. Rev. **117**, 5146 (2017).

[22] I. Rajapaksa, K. Uenal, and H. K. Wickramasinghe, Image force microscopy of molecular resonance: A microscope principle, Appl. Phys. Lett. **97**, 073121 (2010).

[23] J. Jahng, E. O. Potma, and E. S. Lee, Tip-enhanced thermal expansion force for nanoscale chemical imaging and spectroscopy in photoinduced force microscopy, Anal. Chem. **90**, 11054 (2018).

[24] B. T. O'Callahan, J. Yan, F. Menges, E. A. Muller, and M. B. Raschke, Photoinduced tip–sample forces for chemical nanoimaging and spectroscopy, Nano Lett. **18**, 5499 (2018).

[25] See Supplemental Material at http://link.aps.org/supplemental/10.1103/PhysRevApplied.16.014048 for more information regarding the experimental details, additional AFM-IR and micro-FTIR results, the details about AFM-IR sensitivity calculation, and the description of the base spectral components.

[26] A. Berndt, O. Yizhar, L. A. Gunaydin, P. Hegemann, and K. Deisseroth, Bi-stable neural state switches, Nat. Neurosci. **12**, 229 (2009).

[27] I. Amenabar, S. Poly, W. Nuansing, E. H. Hubrich, A. A. Govyadinov, F. Huth, R. Krutokhvostov, L. Zhang, M. Knez, J. Heberle, A. M. Bittner, and R. Hillenbrand, Structural analysis and mapping of individual protein complexes by infrared nanospectroscopy, Nat. Commun. **4**, 1 (2013).

[28] L. Tetard, A. Passian, R. H. Farahi, T. Thundat, and B. H. Davison, Opto-nanomechanical spectroscopic material characterization, Nat. Nanotechnol. **10**, 870 (2015).

[29] A. G. Lee, How lipids affect the activities of integral membrane proteins, Biochim. Biophys. Acta, Biomembr. **1666**, 62 (2004).

[30] E. Ritter, L. Puskar, F. J. Bartl, E. F. Aziz, P. Hegemann, and U. Schade, Time-resolved infrared spectroscopic techniques as applied to channelrhodopsin, Front. Mol. Biosci. **2**, 38 (2015).

[31] A. Barth, Infrared spectroscopy of proteins, Biochim. Biophys. Acta, Biomembr. **1767**, 1073 (2007).

[32] L. K. Tamm and S. A. Tatulian, Infrared spectroscopy of proteins and peptides in lipid bilayers, Q. Rev. Biophys. **30**, 365 (1997).

[33] J. Lombard, P. López-García, and D. Moreira, The early evolution of lipid membranes and the three domains of life, Nat. Rev. Microbiol. **10**, 507 (2012).

[34] E. Ritter, P. Piwowarski, P. Hegemann, and F. J. Bartl, Light-dark adaptation of channelrhodopsin C128T mutant, J. Biol. Chem. **288**, 10451 (2013).

[35] K. Nikolic, N. Grossman, M. S. Grubb, J. Burrone, C. Toumazou, and P. Degenaar, Photocycles of channelrhodopsin-2, Photochem. Photobiol. **85**, 400 (2009).

[36] V. A. Lórenz-Fonfría, T. Resler, N. Krause, M. Nack, M. Gossing, G. F. V. Mollard, C. Bamann, E. Bamberg, R. Schlesinger, and J. Heberle, Transient protonation changes in channelrhodopsin-2 and their relevance to channel gating, Proc. Natl. Acad. Sci. U. S. A. **110**, E1273 (2013).

[37] E. Ritter, K. Stehfest, A. Berndt, P. Hegemann, and F. J. Bartl, Monitoring light-induced structural changes of channelrhodopsin-2 by UV-visible and Fourier transform infrared spectroscopy, J. Biol. Chem. **283**, 35033 (2008).

[38] M. Elgeti, E. Ritter, and F. J. Bart, New insights into light-induced deactivation of active rhodopsin by SVD and global analysis of time-resolved UV/Vis- and FTIR-data, Z. Phys. Chem. **222**, 1117 (2008).

[39] R. Chikkaraddy, B. de Nijs, F. Benz, S. J. Barrow, O. A. Scherman, E. Rosta, A. Demetriadou, P. Fox, O. Hess, and J. J. Baumberg, Single-molecule strong coupling at room temperature in plasmonic nanocavities, Nature **535**, 127 (2016).

[40] F. Huth, A. Chuvilin, M. Schnell, I. Amenabar, R. Krutokhvostov, S. Lopatin, and R. Hillenbrand, Resonant antenna probes for tip-enhanced infrared near-field microscopy, Nano Lett. **13**, 1065 (2013).